Detections of [C II] 158 μm and [O III] 88 μm in a Local Lyman Continuum Emitter, Mrk 54, and Its Implications to High-redshift ALMA Studies[*]

Ryota Ura[1], Takuya Hashimoto[1,2], Akio K. Inoue[3,4], Dario Fadda[5], Matthew Hayes[6], Johannes Puschnig[6,7], Erik Zackrisson[8], Yoichi Tamura[9], Hiroshi Matsuo[10,11], Ken Mawatari[10], Yoshinobu Fudamoto[4,10], Masato Hagimoto[9], Nario Kuno[1,2], Yuma Sugahara[4,10], Satoshi Yamanaka[12], Tom J. L. C. Bakx[9,13], Yurina Nakazato[14], Mitsutaka Usui[1], Hidenobu Yajima[1,15], and Naoki Yoshida[14,16]

[1] Division of Physics, Faculty of Pure and Applied Sciences, University of Tsukuba, Tsukuba, Ibaraki 305-8571, Japan; hashimoto.takuya.ga@u.tsukuba.ac.jp
[2] Tomonaga Center for the History of the Universe (TCHoU), Faculty of Pure and Applied Sciences, University of Tsukuba, Tsukuba, Ibaraki 305-8571, Japan
[3] Department of Physics, School of Advanced Science and Engineering, Waseda University, 3-4-1, Okubo, Shinjuku, Tokyo 169-8555, Japan
[4] Waseda Research Institute for Science and Engineering, Faculty of Science and Engineering, Waseda University, 3-4-1, Okubo, Shinjuku, Tokyo 169-8555, Japan
[5] SOFIA Science Center, Universities Space Research Association, MS 232-11, Moffett Field, CA 94035, USA
[6] The Oskar Klein Centre, Department of Astronomy, Stockholm University, AlbaNova, SE-10691 Stockholm, Sweden
[7] Argelander-Institut für Astronomie, Auf dem Hügel 71, D-53121, Bonn, Germany
[8] Observational Astrophysics, Department of Physics and Astronomy, Uppsala University, Box 516, SE-751 20 Uppsala, Sweden
[9] Department of Physics, Graduate School of Science, Nagoya University, Nagoya 464-8602, Japan
[10] National Astronomical Observatory of Japan, 2-21-1 Osawa, Mitaka, Tokyo 181-8588, Japan
[11] Graduate University for Advanced Studies (SOKENDAI), 2-21-1 Osawa, Mitaka, Tokyo 181-8588, Japan
[12] General Education Department, National Institute of Technology, Toba College, 1-1, Ikegami-cho, Toba, Mie 517-8501, Japan
[13] National Astronomical Observatory of Japan, 2-21-1, Osawa, Mitaka, Tokyo, Japan
[14] Department of Physics, School of Science, The University of Tokyo, 7-3-1 Hongo, Bunkyo, Tokyo 113-0033, Japan
[15] Center for Computational Sciences, University of Tsukuba, Ten-nodai, 1-1-1 Tsukuba, Ibaraki 305-8577, Japan
[16] Kavli Institute for the Physics and Mathematics of the Universe (WPI), UT Institute for Advanced Study, The University of Tokyo, Kashiwa, Chiba 277-8583, Japan

Abstract

We present integral field, far-infrared (FIR) spectroscopy of Mrk 54, a local Lyman continuum emitter, obtained with FIFI-LS on the Stratospheric Observatory for Infrared Astronomy. This is only the second time, after Haro 11, that [C II] 158 μm and [O III] 88 μm spectroscopy of the known LCEs have been obtained. We find that Mrk 54 has a strong [C II] emission that accounts for ~1% of the total FIR luminosity, whereas it has only moderate [O III] emission, resulting in the low [O III]/[C II] luminosity ratio of 0.22 ± 0.06. In order to investigate whether [O III]/[C II] is a useful tracer of f_{esc} (LyC escape fraction), we examine the correlations of [O III]/[C II] and (i) the optical line ratio of $O_{32} \equiv$ [O III] 5007 Å/[O II] 3727 Å, (ii) specific star formation rate, (iii) [O III] 88 μm/[O I] 63 μm ratio, (iv) gas-phase metallicity, and (v) dust temperature based on a combined sample of Mrk 54 and the literature data from the Herschel Dwarf Galaxy Survey and the LITTLE THINGS Survey. We find that galaxies with high [O III]/[C II] luminosity ratios could be the result of high ionization (traced by O_{32}), bursty star formation, high ionized-to-neutral gas volume filling factors (traced by [O III] 88 μm/[O I] 63 μm), and low gas-phase metallicities, which is in agreement with theoretical predictions. We present an empirical relation between the [O III]/[C II] ratio and f_{esc} based on the combination of the [O III]/[C II] and O_{32} correlation, and the known relation between O_{32} and f_{esc}. The relation implies that high-redshift galaxies with high [O III]/[C II] ratios revealed by the Atacama Large Millimeter/submillimeter Array may have $f_{esc} \gtrsim 0.1$, significantly contributing to the cosmic reionization.

Unified Astronomy Thesaurus concepts: Far infrared astronomy (529); Dwarf galaxies (416); Markarian galaxies (1006)

1. Introduction

Studying high-redshift ($z \gtrsim 6$) galaxies at the epoch of reionization (EoR) is essential to understand cosmic reionization. An important parameter of galaxies necessary to understand cosmic reionization is the Lyman continuum (LyC) escape fraction, f_{esc}, which indicates the fraction of ionizing photons ($\lambda \leqslant 912$ Å) in a galaxy that escapes from the galaxy into the intergalactic medium (IGM; e.g., Inoue et al. 2006; Robertson et al. 2013; Robertson 2022).

Numerous efforts have been made to directly observe LyC. Space telescopes such as FUSE and HST identified LyC in more than ~100 galaxies in the local and nearby universe at $z \lesssim 0.4$, and measured f_{esc} ranging from a few percent to more than 70% (e.g., Deharveng et al. 2001; Bergvall et al. 2006; Leitet et al. 2011, 2013; Borthakur et al. 2014; Izotov et al. 2016a, 2016b; Leitherer et al. 2016; Puschnig et al. 2017; Izotov et al. 2018; Wang et al. 2019; Flury et al. 2022a). At higher redshift, spectroscopic detections of LyC in individual galaxies are limited so far. An AstroSat spectroscopically identified LyC in a $z = 1.42$ galaxy, whose f_{esc} is constrained to be higher than 20% (Saha et al. 2020). Large ground-based telescopes such as Keck, VLT, and GTC spectroscopically identified LyC in ~20 individual galaxies at $z \sim 3$–4 with f_{esc} ranging from a few percent to 90% (e.g., de Barros et al. 2016; Shapley et al. 2016; Vanzella et al. 2018; Marques-Chaves et al. 2021; Pahl et al. 2021;

Marques-Chaves et al. 2022). Complementary to these individual spectroscopic detections, there are spectroscopic and imaging surveys at $z \sim 3$–4 that statistically targeted the LyC radiation from galaxies. On the spectroscopy side, the Keck Lyman Continuum Spectroscopic Survey targeted LyC from 124 galaxies at $z \sim 3.1$, and obtained a sample average f_{esc} of $6\% \pm 1\%$ (Steidel et al. 2018; Pahl et al. 2021). On the imaging side, using narrow-band filters that are free from non-ionizing photons, one can observe LyC from galaxies with large ground-based telescopes such as Subaru, VLT, and Keck (e.g., Inoue et al. 2005; Iwata et al. 2009; Nestor et al. 2011; Micheva et al. 2017; Iwata et al. 2019). Compared to spectroscopic surveys, narrow-band imaging observations can efficiently target LyC owing to large fields of view. However, ground-based imaging data can be affected by chance overlap with foreground interlopers (e.g., Vanzella et al. 2010; Nestor et al. 2013). To mitigate such interlopers, Iwata et al. (2019) combined the narrow-band imaging data of Subaru with the high angular resolution imaging data of the Hubble Space Telescope (HST) data. The authors obtained $f_{esc} < 8\%$ (3σ) in a sample of 103 and eight star-forming galaxies and active galactic nuclei (AGNs) with spectroscopic redshifts at $3.06 < z < 3.5$ and 157 photometrically selected $z = 3.1$ Lyα-emitting galaxies. In addition to the narrow-band imaging surveys, Fletcher et al. (2019) and Begley et al. (2022) used broadband filters to target LyC in samples of 61 and 148 galaxies at $z \sim 3.1$ and 3.5, respectively, and obtained an average f_{esc} of 20% and $7\% \pm 2\%$ (see also, e.g., Jones et al. 2021; Saxena et al. 2022a; Rivera-Thorsen et al. 2022). At $z > 4$, it is virtually impossible to directly observe LyC due to absorption by the intervening IGM (Inoue & Iwata 2008). Therefore, it becomes important to establish a link between f_{esc} and other observables at $z = 0$–4, which allows us to indirectly estimate how EoR galaxies have contributed to reionization.

Possible signatures of LyC leakage include (i) a small separation of a double-peaked Lyα profile (e.g., Verhamme et al. 2015; Dijkstra et al. 2016; Kakiichi & Gronke 2021), (ii) intense far-ultraviolet (FUV) emission lines such as Lyα (e.g., Steidel et al. 2018; Flury et al. 2022b; Naidu et al. 2022), C IV 1550 Å (e.g., Saxena et al. 2022b; Schaerer et al. 2022), and Mg II doublet lines at $\lambda\lambda 2796$, 2803 (e.g., Henry et al. 2018; Chisholm et al. 2020), (iii) a high ionization parameter traced by the optical line ratio [O III] 5007 Å/[O II] 3727 Å (O_{32}, e.g., Jaskot & Oey 2013; Nakajima & Ouchi 2014), (iv) a high star formation rate (SFR) surface density (Flury et al. 2022b), (v) a blue UV continuum slope (e.g., Yamanaka et al. 2020; Chisholm et al. 2022), (vi) and a weak equivalent width of low-ionization metal absorption lines (e.g., Jones et al. 2013; Chisholm et al. 2018) as well as a weak low-ionization optical metal emission lines such as [S II] at $\lambda\lambda 6717$, 6731 (Wang et al. 2019). On the whole, the LyC escape appears to depend on H I column density, ionization parameter, and stellar feedback (Flury et al. 2022b), as also predicted by theoretical studies (see, e.g., Yajima et al. 2011; Zackrisson et al. 2013; Yajima et al. 2014; Ma et al. 2015; Paardekooper et al. 2015; Arata et al. 2019; Barrow et al. 2020; Rosdahl et al. 2022; Yeh et al. 2023).

In addition to these techniques, Katz et al. (2020, 2022) propose the far-infrared (FIR) line luminosity ratios of [O III] 88 μm and [C II] 158 μm (hereafter, [O III]/[C II]) as a new diagnostic signature of LyC escape. This is motivated by spectroscopic observations of $z = 6$–9 galaxies with the Atacama Large Millimeter/submillimeter Array (ALMA;

Inoue et al. 2016; Laporte et al. 2017; Hashimoto et al. 2018; Tamura et al. 2019). Inoue et al. (2016) observed a $z = 7.2$ Lyα-emitting galaxy in [O III] 88 μm and [C II] 158 μm, and obtained a high line luminosity ratio [O III]/[C II] $\gtrsim 12$ (3σ). With a simple one-dimensional photoionization model, the authors for the first time proposed that the high line ratio may indicate a high f_{esc} because a weak [C II] emission could be linked to a low amount of H I gas in the interstellar medium (ISM). Hashimoto et al. (2019) compiled a sample of galaxies with [O III]/[C II] at $z > 6$, and found that UV-selected galaxies in the EoR typically show [O III]/[C II] ~ 3–10 or higher (see also Laporte et al. 2019; Bakx et al. 2020; Carniani et al. 2020; Harikane et al. 2020; Witstok et al. 2022). These values are higher than the typical values of local spirals (~ 0.5; Brauher et al. 2008) and low-metallicity dwarf galaxies (~ 2; Madden et al. 2013; Cormier et al. 2015) observed by ISO and Herschel, respectively, suggesting unusual conditions of the ISM in high-z galaxies (e.g., Sugahara et al. 2022).

Using the photoionization models of CLOUDY constructed by Ferland et al. (2013); Harikane et al. (2020) showed that these high [O III]/[C II] ratios can be explained by combinations of various parameters such as a high ionization parameter, low neutral gas covering fraction in the ISM, low gas density, and high O/C abundance ratio, where the scenarios of high ionization parameter and low neutral gas covering fraction would facilitate the LyC escape. In addition, Vallini et al. (2021) theoretically parameterized the [O III]/[C II] ratio as a function of the burstiness of star formation activity, gas density, and metallicity. The authors found that the parameter mostly affecting the line ratio is the burstiness. More recently, Ramambason et al. (2022) examined ISM properties of a local sample of the Herschel Dwarf Galaxy Survey (HDGS; Madden et al. 2013; Cormier et al. 2015) using a grid of models of H II regions and photodissociated regions. The authors also found a positive correlation between [O III]/[C II]and predicted f_{esc}. Although many parameters are degenerate, the fact that the EoR UV-selected galaxies show on average high [O III]/[C II] luminosity ratios is interesting because it may suggest high f_{esc} values. It is crucial to observationally link the luminosity ratios to f_{esc}, as done with other techniques, as well as to understand the characteristics of galaxies with high [O III]/[C II] ratios. If such correlations are established in the local universe, we can apply them to the EoR galaxies observed with ALMA to indirectly infer their properties, including f_{esc}. Unfortunately, only for one known local Lyman continuum emitter (LCE), Haro 11 (e.g., Hayes et al. 2007; Leitet et al. 2011), the [O III]/[C II] ratio has been observed (~ 2.0 in Cormier et al. 2015). The reason for the paucity of local LCEs with FIR line observations is that most LCEs were discovered after 2013, when Herschel ended its operations.

The Stratospheric Observatory for Infrared Astronomy (SOFIA) offered a unique opportunity to perform FIR line spectroscopy of local galaxies. Here, we report observations of the FIR lines in Mrk 54 using FIFI-LS (Field-Imaging Far-Infrared Line Spectrometer, Fischer et al. 2018) on board SOFIA; Mrk 54 is the second nearest galaxy after Haro 11 with a direct LyC detection at a luminosity distance of ~ 191 Mpc. The galaxy is a blue compact galaxy with $12 + \log(O/H) = 8.6$, SFR $= 12\,M_\odot$ yr^{-1}, $f_{esc} = 2.5\%$ (Leitherer et al. 2016) and $O_{32} = 0.4$ (Chisholm et al. 2018). These two well-characterized LCEs with FIR line spectroscopy, Haro 11 and Mrk 54, are

invaluable to calibrating an observational relationship between [O III]/[C II] and f_{esc}. Because [O III]/[C II] depends on various parameters, we also make use of local analogs of high-z galaxies with FIR line spectroscopy (e.g., low stellar mass or gas-phase metallicity), the HDGS and the LITTLE THINGS Survey (LT; Hunter et al. 2012; Cigan et al. 2016, 2021), to statistically examine the correlations between [O III]/[C II] and other physical quantities such as ionization parameter, ionized-to-neutral gas volume filling factor, gas-phase metallicity, and burstiness. In light of recent combined observations of high-z galaxies with ALMA and JWST in the rest-frame optical and FIR (e.g., Bakx et al. 2023), respectively, the presented study will be a reference study that is useful (1) to infer f_{esc} of galaxies in the EoR and (2) to plan and interpret the ALMA +JWST observations (e.g., Kohandel et al. 2023; Nakazato et al. 2023).

This paper is structured as follows. In Section 2, we present the SOFIA observations and data reduction of Mrk 54. In Section 3, we summarize the physical properties of the two literature samples of HDGS and LT. In Section 3, we present analyses of statistical correlations between [O III]/[C II] and other physical quantities. In Section 5, we establish a relation between [O III]/[C II] and f_{esc}, and apply it to high-z ALMA galaxies. We summarize our conclusions in Section 6. Throughout this paper, we assume a Lambda cold dark matter cosmology with $\Omega_m = 0.272$, $\Omega_b = 0.045$, $\Omega_\Lambda = 0.728$, and $H_0 = 70.4$ km s^{-1} Mpc^{-1} (Komatsu et al. 2011). We use $L_\odot = 3.839 \times 10^{33}$ erg s^{-1} as solar luminosity and 12+log(O/H) = 8.7 as solar metallicity (Asplund et al. 2009).

2. SOFIA Observations and Data Reduction

Mrk 54 was observed by the SOFIA FIFI-LS (Fischer et al. 2018) during cycles 7 and 8 (PIDs: 07_0108 and 08_0063, PI: T. Hashimoto). FIFI-LS has two parallel spectral channels that cover $1' \times 1'$ in the wavelength ranges of 115–203 μm (*red channel*) and $0'.5 \times 0'.5$ in the ranges of 51–125 μm (*blue channel*), split into 5×5 spatial pixels. The red and blue channels were used to target the [C II] 158 μm and [O III] 88 μm lines. The two observations were executed on 2020 February and 2021 May for a total on-source exposure time of 2426 s. The target galaxy Mrk 54 was entirely covered by a single field of view. The observations were performed in symmetric chopping mode with a 120$''$ chop amplitude. A spatial dithering pattern was used to cover regions with bad pixels and to better recover the spatial resolution of the instrument. Eight grating positions were used to slightly extend the spectral coverage and to oversample the wavelength range in order to compensate for bad pixels and to better define the line profiles.[17]

At the wavelengths of [C II] 158 μm and [O III] 88 μm lines, the spatial resolution is approximately 15$''$.6 and 8$''$.8, the instantaneous spectral coverage is 1560 and 2340 km s^{-1}, and the spectral resolution is 260 and 490 km s^{-1}. Further details on FIFI-LS can be found in Fischer et al. (2018) and Colditz et al. (2020).

Data reduction was carried out using the FIFI-LS data reduction pipeline (Vacca et al. 2020) combining the two sets of data taken in cycles 7 and 8. The flux calibration, which is performed using sky calibrators, has an absolute uncertainty of

less than 20%. Hereafter, we only consider the measurement uncertainties. The data were corrected for the atmospheric absorption with a transmission curve modeled with ATRAN (Lord 1992), using precipitable water vapor values measured during the flight. The final cubes were sampled on a grid with spatial pixels of 3$''$ and 1$''$.5 (a fourth of the original pixels) and spectral pixels of 32.5 and 61.25 km s^{-1} (oversample of a factor of 8 in spectral resolution) for the red and blue array, respectively.

The data were analyzed with the SOFIA SPectral EXplorer (sospex, Fadda & Chambers 2018). We first obtained a pure line cube by subtracting the dust continuum level from the spectral cube at each spatial pixel. We then defined an elliptical aperture by co-adding the cube along the wavelength dimension and considering ellipses centered on the flux centroid of this image. Major and minor axes were optimized by selecting the smallest ellipse containing the asymptotic value of total flux. Finally, we extracted the spectrum within this elliptical aperture and fit a Gaussian function to the line to estimate total flux, central wavelength, and FWHM.

The top left (right) panel of Figure 1 shows the [C II] ([O III]) intensity map with contours of the Pan-STARRS i-band image, whereas the bottom left (right) panel depicts the corresponding [C II] ([O III]) spectrum extracted from the aperture. The [C II] ([O III]) line is detected at a significance level of 24σ (4σ) integrated over the line profile, where 1σ corresponds to the typical uncertainty per spectral bin measured in the spectrum as indicated by the horizontal dashed lines.[18]

Motivated by recent observations of high-z galaxies that demonstrated that [C II] is spatially extended compared with [O III] (e.g., Carniani et al. 2017; Fujimoto et al. 2019; Vallini et al. 2021; Witstok et al. 2022), we examined the spatial sizes of these emission lines in Mrk 54 with the surface brightness profiles. We found that [O III] is barely resolved with an upper limit of the intrinsic size of 8$''$.8, whereas [C II] is only marginally resolved with an intrinsic size of 7$''$.9. Thus, we do not find clear evidence of spatially extended [C II] emission in Mrk 54 at the FIFI-LS's spatial resolution.

With sospex, we found that [C II] and [O III] have the line fluxes of (4.68 ± 0.16) and $(1.01 \pm 0.27) \times 10^{-16}$ W m^{-2}, FWHMs of 329 ± 13 and 292 ± 90 km s^{-1}, and redshifts of 0.04497 ± 0.00002 and 0.0443 ± 0.0001, respectively. The [C II] and [O III] redshift is consistent with that of the optical redshift, 0.0447 ± 0.0002 (Deharveng et al. 2001), within 1σ and 2σ uncertainties, respectively. The corresponding [C II] and [O III] luminosities are (5.90 ± 0.21) and $(1.27 \pm 0.34) \times 10^8 L_\odot$, respectively.

2.1. Comparisons of Line Luminosities to the Literature Samples

The left (right) panel of Figure 2 compares the FIR and [C II] ([O III]) luminosity of Mrk 54 with a compiled sample of the literature, where the FIR luminosity of Mrk 54 is obtained from photometry with IRAS 60 and 100 μm as in Helou et al. (1985). The literature sample first includes the data points of Herrera-Camus et al. (2018), a compilation of local H II galaxies, LINER, Seyfert, and high-z galaxies. The literature

---

[17] We only use wavelengths observed at 80% or more of the time relative to the total observation time.

[18] We measured the noise level per spectral bin, and adopted the standard deviation of the distribution as the 1σ value. We used the wavelength ranges of [164.42, 164.60] and [165.02, 165.17] μm for [C II], whereas [92.04, 92.15] and [92.43, 92.65] μm for [O III]. In this estimate, we neglected the wavelength dependence of the noise level for simplicity.
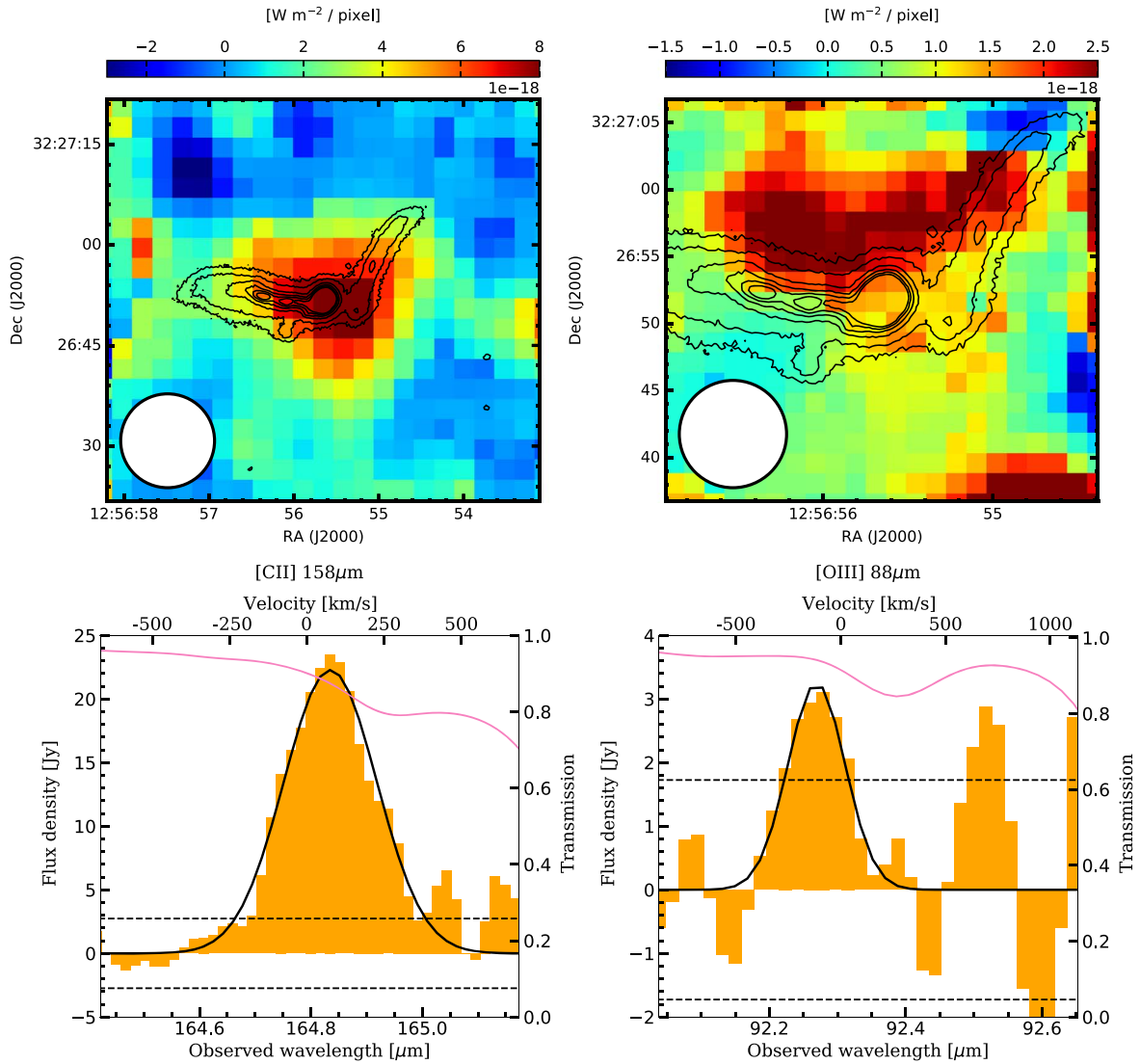
Figure 1. Top left and right panels show the intensity maps of [C II] and [O III] as the colored background, respectively, with flux scales denoted in the scale bar. In each panel, the black contours depict the morphology of Mrk 54 in the Pan-STARRS i-band image. Note that the left and right panels do not have the same physical scale because of the different fields of view. The circles at the bottom left corners indicate the beam size of FIFI-LS. Bottom left and right panels show the spectra of [C II] and [O III], respectively. In each panel, the magenta curve indicates the atmospheric transmission curve convolved with the spectral resolution of FIFI-LS. The black solid line shows the best-fit Gaussian profile to the line, whereas the horizontal black dashed line shows the typical 1σ uncertainty. In the top x-axis, the velocity zero-point is defined at $z = 0.0447$ (Deharveng et al. 2001).

data also include a subsample of the Lyman Alpha Reference Sample (LARS; Hayes et al. 2013), $z \sim 0.03$–0.18 galaxies characterized by its ongoing starburst and Lyα emission. Seven and two of the LARS galaxies were observed in [C II] and [O III], respectively (Puschnig et al. 2020). Finally, we also include the literature data points of Smirnova-Pinchukova et al. (2019), a subsample of five nearby luminous Seyfert 1 AGN host galaxies observed in [C II]. Interestingly, Mrk 54 has strong [C II] emission that accounts for as high as $\sim 1\%$ of the FIR luminosity, whereas it has only moderate [O III] emission. Based on the two line luminosities, we obtain [O III]/[C II] $= 0.22 \pm 0.06$, much lower than those obtained in another LCE, Haro 11 (~ 2) and high-z ALMA galaxies (~ 3–10).

Strong [C II] emission in Mrk 54 could be due to the presence of outflow as discussed in, e.g., Smirnova-Pinchukova et al. (2019) and Puschnig et al. (2020). Alternatively, previous theoretical works have shown that FIR line luminosity ratios can be affected by the presence of X-ray-dominated regions in

AGNs (e.g., Meijerink et al. 2007; Wolfire et al. 2022). Nevertheless, observational studies of Decarli et al. (2022) and Walter et al. (2018) demonstrated that the FIR line ratios can be reasonably reproduced by the photodissociated region models, indicating that the presence of hidden AGN activity in Mrk 54, if any, may not be the primary cause of the strong [C II] emission.

2.2. Spatial and Velocity Offsets of [C II] and [O III] in Mrk 54

Figure 3 shows a direct comparison of the spatial distributions of [O III], [C II], and the i-band position of Mrk 54 in the field of view of [O III], where the contours are drawn to show the flux centroids. We find that the [C II] flux centroid matches the i-band position of Mrk 54, whereas the [O III] flux centroid is spatially offset by $\sim 5''$ (~ 4 kpc). In the case of weak detections, the centroid of a point source is not well defined since almost no flux is detected in the adjacent pixels. Nevertheless, the position of the center of the emission can be
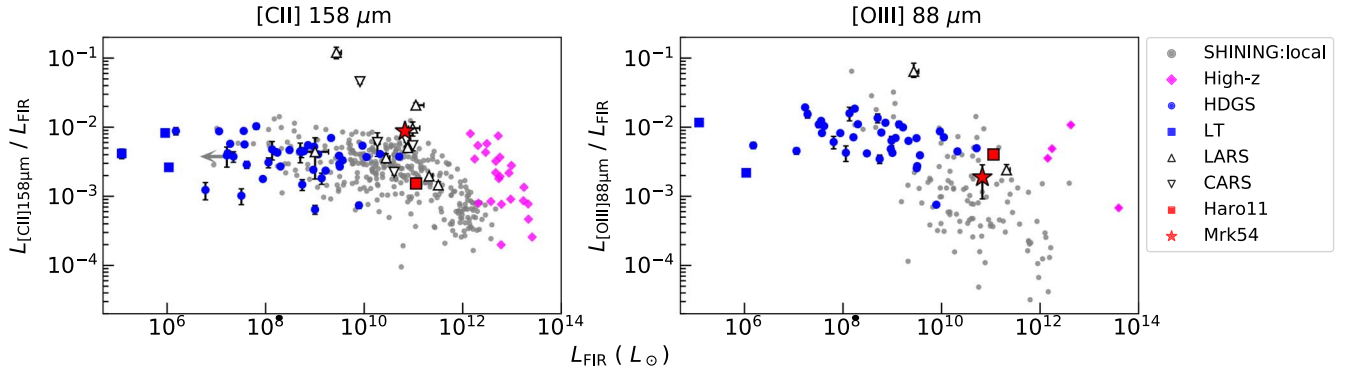
Figure 2. Left and right panels show [O III]- and [C II]-to-FIR line luminosity ratios, $L_{[C\ II]}/L_{FIR}$ and $L_{[O\ III]}/L_{FIR}$ plotted against L_{FIR}, respectively. In each panel, Mrk 54 and Haro 11 are indicated by a red star and square with measurement uncertainties, respectively. Gray circles and magenta diamonds indicate the compilation of the FIR line observations of local and high-z objects, respectively, from Herrera-Camus et al. (2018), where the local sample includes H II galaxies, LINER, and Seyfert. The blue circles and squares show the data points of HDGS (Cormier et al. 2012) and LT (Cigan et al. 2016). The upward and downward triangles indicate a subsample of local galaxies from the LARS (Puschnig et al. 2020) and CARS projects (Smirnova-Pinchukova et al. 2019) with the FIR line observations, some of which are characterized by enhanced FIR emission. Mrk 54 has strong [C II] emission, whereas it has moderate [O III] emission.
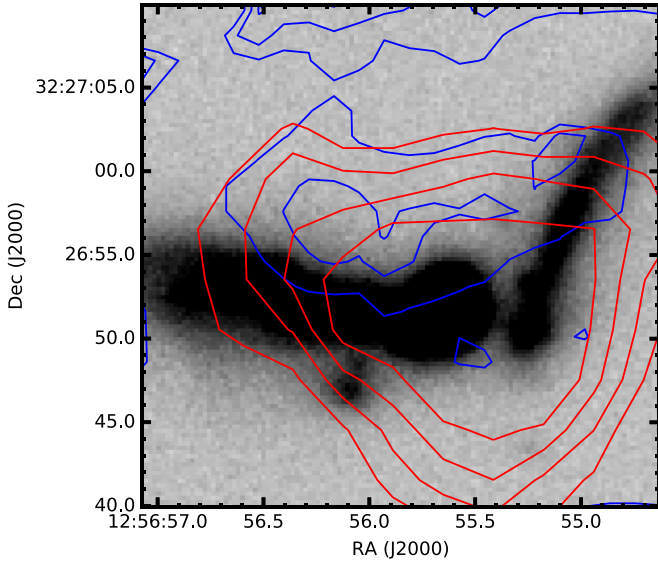
Figure 3. Comparisons of the spatial distributions of [C II], [O III], and the Pan-STARRS i-band image. Red and blue contours indicate the spatial distributions of [C II] and [O III], respectively, with the Pan-STARRS i-band image as the background. The contours are drawn at equal intervals with an arbitrary unit for display purposes.

reconstructed using spatial dithering as done in our observations. Another possible cause of mismatch is a misalignment of the blue and red arrays since the two spectra are acquired simultaneously. This is possible only if the rotation of the K-mirror of FIFI-LS (see Colditz et al. 2020), the beam rotator that rotates the instrument's field of view counteracting the sky rotation experienced by the SOFIA telescope, is not accurately taken into account during the observation. The K-mirror parameters are measured before each FIFI-LS series since the cooling of the instrument slightly modifies its optical path. Since there are no similar issues with other observations in the two series when Mrk 54 was observed we can also exclude this possibility. Finally, we notice that the peak of the [O III] emission is detected in the same position in the two independent observations obtained in the two different FIFI-LS series. This strongly suggests that the detection is real as well as the difference in position with respect to the peak of the [C II] emission.

Interestingly, similar spatial offsets among the [C II], [O III], and rest-frame UV continuum emitting regions were observed in galaxies in the EoR; Carniani et al. (2017) showed a spatial offset in each of [C II], [O III], and the rest-frame UV stellar continuum in a $z = 7.11$ galaxy, BDF-3229 (see also Laporte et al. 2019). More specifically, the galaxy shows a 4 kpc offset between the UV stellar continuum and [C II] regions, and 1–30 kpc offset between the [C II] and [O III] emitting regions.[19] Furthermore, in the local universe, Cigan et al. (2016) have shown a spatial offset of [O III] and [C II] in local metal-poor dwarf galaxies, DDO 69 and DDO 70, although the offsets are as small as 0.1–0.2 kpc. From the theoretical viewpoint, based on cosmological hydrodynamic simulations combined with radiative transfer calculations, Katz et al. (2019) have shown that the spatial offsets of [C II] and [O III] can be caused by a clumpy structure due to, e.g., merger events, presence of small satellites, or a fragmented disk (see also Vallini et al. 2017 for another explanation of the spatial offset due to the stellar photoevaporation feedback effect). Similarly, based on cosmological hydrodynamic simulations implementing the photoionization models of CLOUDY, Moriwaki et al. (2018) have shown that there can be a spatial offset between [O III] 88 μm and the rest-frame optical continuum that traces the distribution of the bulk stellar population (see their Figure 3). The spatial offset could be due to the fact that the rest-frame optical continuum traces the older stellar population, whereas the [O III] 88 μm traces the outer region of the actively star-forming regions (K. Moriwaki, private communication). These studies support the claim that the [O III] emission in Mrk 54 could be real. Hereafter, we treat the [O III] detection as real. We stress that the [O III]/[C II] ratio in Mrk 54 remains low even if [O III] is considered undetected.

Finally, we note that the [C II] line is redshifted with respect to the [O III] line by 192 ± 30 km s^{-1} in Mrk 54 (Figure 1). At high-z, Carniani et al. (2017) reported that [C II] is blueshifted with respect to [O III] by $\sim$500 km s^{-1} in the BDF-3299 galaxy at $z = 7.2$ (see also, e.g., Algera et al. 2023 for other high-z examples). The authors ascribed the velocity offset to different kinematics of [C II]- and [O III]-emitting gas, i.e., predominantly neutral and the ionized-gas phase, respectively.

---

[19] The BDF-3299 galaxy has three clumps of [O III], whose spatial offset from the [C II] emission varies from 1–30 kpc.

Because Mrk 54 is an LCE, such different kinematics of gas might indicate a hint of LyC photon leakage from galaxies into the surrounding IGM. However, we leave further discussion to future papers because another local LCE, Haro 11, does not show any velocity offset between the [C II] and [O III] lines (Cormier et al. 2015).

3. Literature Samples

For our analysis, we make use of data from HDGS and LT. The HDGS sample consists of 50 local metal-poor dwarf galaxies, including the LCE Haro 11 (Cormier et al. 2012), and it is characterized by low gas-phase metallicity ranging from near solar metallicity down to $12+\log(O/H) = 7.14$. In most cases, these galaxies have PACS spectroscopic observations for both [C II] 158 μm and [O III] 88 μm, followed by [O I] 63 μm and weaker lines of [O I] 145 μm and [N II] 122/205 μm, in addition to PACS imaging. The sample also includes measurements of various ancillary multiwavelength photometric (UV to radio) and spectroscopic data, best suitable for examining the correlation between the [O III]/[C II] line luminosity ratios and other observables or physical quantities. Specifically, we examine the correlations against (i) the ionization parameter, U_{ion}, traced by $O_{32} \equiv [O III] 5007 Å / [O II] 3727 Å$, (ii) specific SFR defined as the SFR per unit stellar mass, sSFR, (iii) dust temperature, T_{dust}, (iv) ionized-to-neutral gas fraction traced by the [O III] 88 μm-to-[O I] 63 μm line ratio, and (v) the gas-phase metallicity in units of $12+\log(O/H)$. The choice of these parameters is motivated by the theoretical predictions of Vallini et al. (2021) and Katz et al. (2022) except for T_d. The correlation against T_d is considered because Walter et al. (2018) have shown a positive correlation between [O III]/[C II] and T_d (see Figure 4 in their paper).

From the parent sample of 50 galaxies, we first narrow down the sample to 41 galaxies with both [C II] 158 μm and [O III] 88 μm data across the entire galaxy scale. Among these, the numbers of galaxies with O_{32}, sSFR, T_{dust}, FIR [O III]/[O I], and $12+\log(O/H)$ are 18, 36, 33, 35, and 41, respectively. The stellar masses and SFRs are adopted from Madden et al. (2013) and De Looze et al. (2014), respectively.[20] The gas-phase metallicities of the sample are adopted from Madden et al. (2013) and references therein, which are estimated from optical lines. We compute O_{32} in the sample using these literature data.[21] Finally, we adopt T_d of the sample in Rémy-Ruyer et al. (2013) estimated from multiple dust photometry using modified blackbody models.[22] The subsample used in this study has median values of $O_{32} = 5.5$, sSFR = 0.5 Gyr^{-1}, $T_d = 32$ K, FIR [O III]/[O I] = 2.7, and $12+\log(O/H) = 8.0$.

The galaxies in the LT survey share similar properties to the HDGS galaxies such as low gas-phase metallicity, but they are characterized by lower surface brightness and moderate star formation activity. Four LT galaxies in Cigan et al. (2016) were observed in both [C II] and [O III], and have lower [O III]/[C II] luminosity ratios than the HDGS galaxies (Cigan et al. 2016). Thus, the sample is useful to accurately examine the correlation between [O III]/[C II] and $12+\log(O/H)$. The numbers of galaxies with O_{32}, sSFR, T_{dust}, FIR [O III]/[O I], and $12+\log(O/H)$ are 0, 2, 1, 2, and 4, respectively, and the values are adopted from Cigan et al. (2016) and Cigan et al. (2021).

4. Characteristics of High [O III]-to-[C II] Galaxies

We examined the correlation of the [O III]/[C II] line luminosity ratios with other observable quantities using our combined sample, which consists of Mrk 54, HDGS galaxies, including Haro 11 and LT galaxies. We use the Kendall rank correlation test to statistically examine the correlations, where a p-value of 0.05 is used to reject the null hypothesis that the two quantities do not correlate. The correlations and relative Kendall's correlation coefficients are plotted in Figure 4.

The results show that objects with high [O III]/[C II] line luminosity ratios are characterized by high O_{32} (i.e., high U_{ion}), high sSFR (i.e., undergoing a bursty event or a young stellar age), high FIR [O III]/[O I] (i.e., large volume fraction of ionized gas to neutral gas), and low metallicity. The result that high [O III]/[C II] shows high ionization parameters and burstiness is consistent with Harikane et al. (2020), Sugahara et al. (2022), and Algera et al. (2023), respectively. We do not observe a strong correlation between [O III]/[C II] and T_d (but see Walter et al. 2018; Algera et al. 2023). The strongest correlations are found in O_{32} (i.e., U_{ion}) and high FIR [O III]/[O I] (i.e., the ionized-to-neutral gas volume filling factor), which are in qualitative agreement with the claims of Harikane et al. (2020) and Katz et al. (2022). Although we found a correlation between [O III]/[C II] and metallicity, it should be noted that all four LT galaxies have low [O III]/[C II] ratios despite their low metallicity, supporting the claims of Vallini et al. (2021) who showed that the metallicity is not a main factor that changes [O III]/[C II]. The correlations with metallicity and T_d have also been investigated in Cigan et al. (2016), but to our knowledge, this is the first observational study that examines the correlations with O_{32}.

5. Discussion

5.1. [O III]/[C II]–f$_{esc}$ Relation
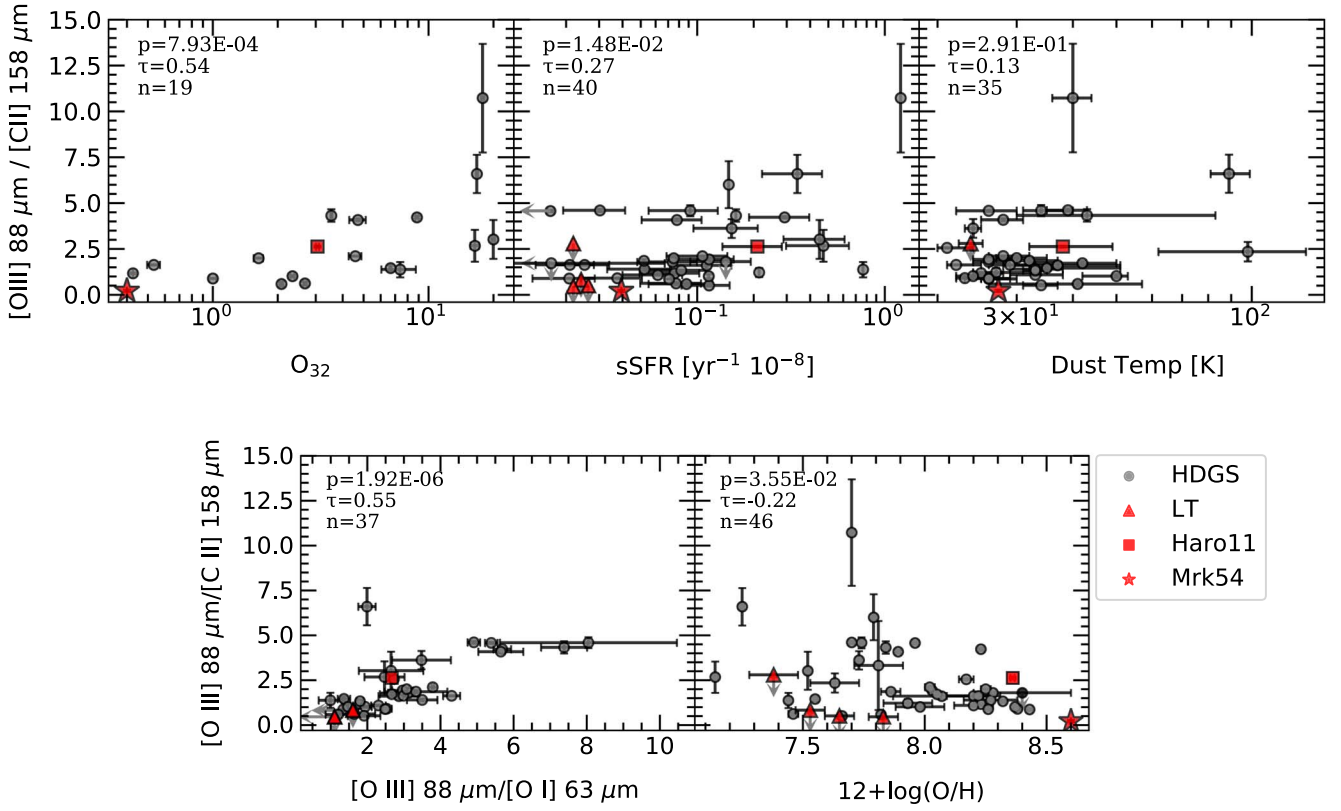
As mentioned in Section 1, a quantitative description of the cosmic reionization process requires estimates of f_{esc} in galaxies in the EoR. We discuss the possibility to use the FIR [O III]/[C II] luminosity ratios to infer f_{esc}.

Based on observations of LCEs and non-LCEs among the local galaxies, Chisholm et al. (2018) derived an equation that links O_{32} to f_{esc} as follows:

$$f_{esc,O_{32}}^{pre} = (0.0017 \pm 0.0004)O_{32}^2 + (0.005 \pm 0.007), \quad (1)$$

where $f_{esc,O_{32}}^{pre}$ is a predicted value of the LyC escape fraction from O_{32} (see also Izotov et al. 2016b). Note that the correlation between f_{esc} and O_{32} has been statistically confirmed in a recent study by Flury et al. 2022b, who significantly increases the sample of LCEs and non-LCEs. Because an equation relating the two quantities is not provided

---

[20] Note that Madden et al. (2013) also reported SFRs estimated from the IR luminosity. Because the sample is expected to be dust-poor, this method can underestimate the SFRs. We thus use the estimates in De Looze et al. (2014) from GALEX FUV and Spitzer/MIPS 24 μm, i.e., SFR(UV+IR). Because De Looze et al. (2014) obtained SFR(UV+IR) for a subsample of the HDGS, we first obtained the relation between SFR(UV) and SFR(UV+IR) in the subsample, and applied a typical correction to the rest of the sample.

[21] The optical line spectroscopy of the sample galaxies was often performed with slit modes around bright star clusters. For fairer comparisons of multiwavelength spectroscopic data, optical integral field unit spectroscopy will be crucial. Note that previous studies that use the HDGS's FIR and optical data also suffer from the same issue (Vallini et al. 2021; Witstok et al. 2022).

[22] Sommovigo et al. (2021) introduced another technique to estimate T_d from the measurements of the [C II] luminosity and continuum flux density at 158 μm. Although we adopt T_d from spectral energy distribution fitting, we expect a similar correlation as the two methods provide consistent dust temperatures (Figure 2 of Sommovigo et al. 2021).

Figure 4. Correlations of [O III]/[C II] line luminosity ratios plotted against O_{32}, sSFR, T_d, the FIR [O III]/[O I] luminosity ratios, and gas-phase metallicity in units of 12+log(O/H). In each panel, the red star and square indicate Mrk 54 and Haro 11, respectively. Gray circles show the HDGS galaxies, whereas the red triangles show the LT galaxies. Note that Mrk 54 does not have a measurement of the FIR [O III]/[O I] line ratio, whereas the LT galaxies do not have measurements of O_{32}. In the upper middle panel, the sSFR values of the LT galaxies are shifted up to 0.1 dex for display purposes. In each panel, the values in the top left corners are the p-value, Kendall's correlation coefficient (τ), and number of galaxies (n) used to examine the correlations.

in Flury et al. (2022b), in this study, we use the relation of Chisholm et al. (2018) for simplicity. As shown in Figure 4, we obtained a positive correlation between optical O_{32} and FIR [O III]/[C II]. If we fit the correlation with a linear function, it can be written as

$$O_{32} = (1.311 \pm 0.010)[\text{O III}]/[\text{C II}] + (-0.384 \pm 0.016),$$
(2)

using a package of `scipy.optimize.curve_fit`. Combining these two equations, we obtain the following equation that relates [O III]/[C II] to f_{esc},

$$\begin{aligned} f_{\text{esc}}^{\text{pre}} = &(0.0029 \pm 0.0007)([\text{O III}]/[\text{C II}])^2 + \\ &(-0.0017 \pm 0.0004)[\text{O III}]/[\text{C II}] + (-0.005 \pm 0.007). \end{aligned}$$
(3)

The positive correlation between the two quantities is in qualitative agreement with the predictions of Inoue et al. (2016), Katz et al. (2022), and Ramambason et al. (2022).

In the left panel of Figure 5, we plot the predicted relation of LyC escape fraction along with the data points of Mrk 54, Haro 11, and POX 186. Mrk 54 and Haro 11 have direct measurements of the LyC escape fraction. Mrk 54 and Haro 11 measured escape fractions of 0.025 ± 0.007 (Leitherer et al. 2016) and 0.033 ± 0.007 (Leitet et al. 2011), whereas the predicted values are $f_{\text{esc}}^{\text{pre}} = 0.005_{-0.005}^{+0.007}$ and 0.021 ± 0.013, respectively. The measured and predicted values in Mrk 54 and Haro 11 are consistent with each other within 2σ and 1σ uncertainties.

In the left panel of Figure 5, a galaxy called POX 186 shows the highest [O III]/[C II] luminosity ratio $\sim$10 among the local galaxies, which corresponds to a high $f_{\text{esc}}^{\text{pre}} \sim (0.32 \pm 0.15)$. Although direct LyC observations are not performed in the galaxy, its intense star formation activity (sSFR $\sim$12 Gyr^{-1}) also supports that the galaxy is a candidate for strong LCE. Recently, Eggen et al. (2021) performed integral field unit observations of optical emission lines, and found evidence of strong ionized gas outflow that can facilitate the LyC escape. The indirect signature of strong LyC escape in POX 186 supports that the FIR [O III]/[C II] ratios can be used at least to search for promising LCE candidates.

5.2. Implications for High-redshift ALMA Studies

We now turn our attention to the results of high [O III]/[C II] luminosity ratios in the UV-selected galaxies at $z \sim 6$–9 (e.g., Hashimoto et al. 2019; Bakx et al. 2020; Harikane et al. 2020; Witstok et al. 2022). In the following, we adopt the latest line luminosity measurements of nine ALMA [O III] 88 μm galaxies at $z \sim 6$–9 from Carniani et al. (2020). The nine galaxies were detected in both emission lines, and have [O III]/[C II] $\sim$ 3–10.[23] The only exception is SXDF-NB1006-2 where we adopt a new measurement of [O III]/[C II] = 6.1–9.6 (Ren et al. 2023).

---

[23] Among the nine high-z galaxies, [C II] has been originally reported to be undetected in SXDF-NB1006-2 (Inoue et al. 2016), A2744-YD4 (Laporte et al. 2019), and MACS1149-JD1 (Laporte et al. 2019). Later, Carniani et al. (2020) reanalyzed the [C II] data and found 4σ detections.
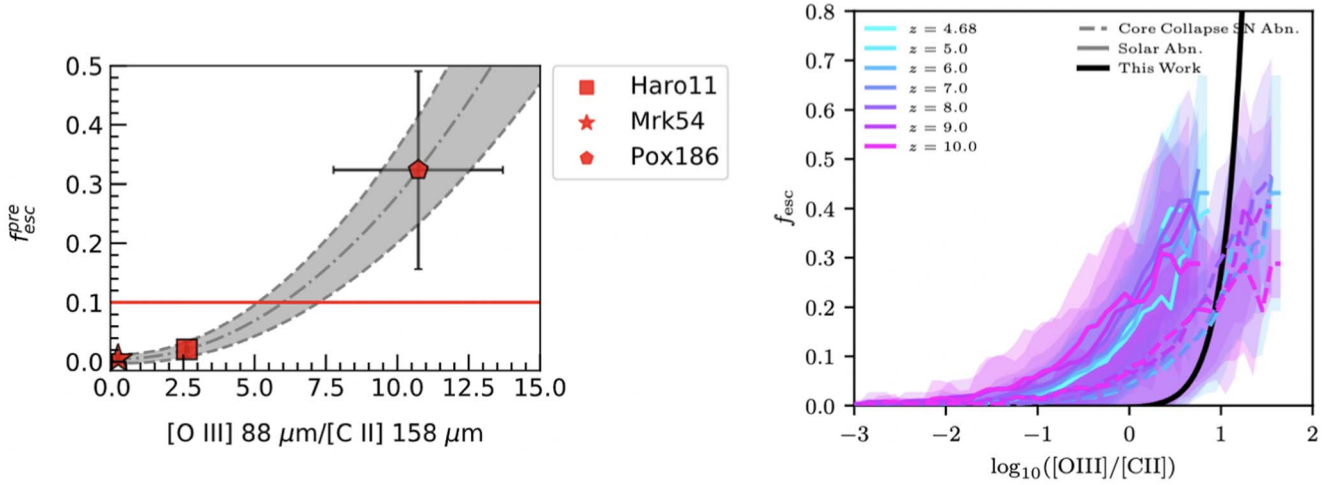
Figure 5. (Left) Predicted value of the LyC escape fraction, f_{esc}^{pre}, obtained from the [O III]/[C II] luminosity ratio using Figure 4. The shaded region indicates the 1σ uncertainty of the [O III]/[C II]–f_{esc}^{pre} relation. The red star and square indicate Mrk 54 and Haro 11, respectively, which have direct measurements of f_{esc}. The red pentagon shows POX 186 with the highest [O III]/[C II] luminosity ratio, ~10, in the local universe. (Right) Comparisons of the best-fit [O III]/[C II]–f_{esc}^{pre} relation (black solid line) and the results of cosmological hydrodynamical simulations in Katz et al. (2022) (colored shaded regions and lines). As in Katz et al. (2022), the colored lines and shaded region indicate the mean relation and 1σ scatter for different redshift bins. The solid and dashed lines represent the results with assumed values of solar abundances and core-collapse supernovae abundances, respectively.

Under the assumption that the same [O III]/[C II]–f_{esc} relation can be applied to these EoR galaxies, the nine high-z ALMA [O III] 88 μm galaxies are expected to have $f_{esc} \sim 0.01$–0.25. In particular, MACS 0416_Y1 at $z=8.31$ (Tamura et al. 2019; Bakx et al. 2020), J0235 at $z=6.0$ (Harikane et al. 2020) and SXDF-NB1006-2 at $z=7.21$ (Inoue et al. 2016; Ren et al. 2023) have [O III]/[C II] $\gtrsim 7$, and could be candidate LCEs with $f_{esc} \gtrsim 0.1$, which is an average value required for galaxies to explain the cosmic reionization process (e.g., Inoue et al. 2006; Finkelstein et al. 2019; Ma et al. 2020).

Based on cosmological hydrodynamical simulations, Katz et al. (2022) obtained a relation between f_{esc}^{pre} and [O III]/[C II] at $z \sim 4$–10. The right panel of Figure 5 shows comparisons of our Equation (3) and the results of cosmological hydrodynamical simulations in Katz et al. (2022) for mock galaxies with SFR $> 10^{-2} M_\odot$ yr^{-1}. If we limit the luminosity ratio range to the observed one of log([O III]/[C II]) ~ 0–1, we find that our best-fit relation systematically predicts lower f_{esc} values. Katz et al. (2022) also presented the f_{esc}^{pre}–[O III]/[C II] relation taking the mass dependence of f_{esc}^{pre} into account (see their Equation (4)). With this relation, the authors obtained escape fractions of 0.005–0.022 in the same nine galaxies at $z=6$–9, even lower than our predictions. These results imply that we also need to take the mass dependence of f_{esc}^{pre} into account. We do note, however, that other observational techniques (e.g., the peak separation of Lyα and O$_{32}$, etc.) usually do not take the mass dependence into account either. As the number of LCEs with [O III]/[C II] is just two, it is impossible to observationally examine the mass dependence of the [O III]/[C II]–f_{esc} relation in a statistical manner. We also note that the stellar masses of high-z galaxies are generally largely uncertain due to the lack of rest-frame optical data. Furthermore, there is observational evidence that massive galaxies do not necessarily have low f_{esc}. Indeed, Marques-Chaves et al. (2021) and Marques-Chaves et al. (2022) have shown that extremely UV luminous and massive (log($M_*/M_\odot$) $\sim 9.9 \pm 0.1$) galaxies have significant LyC escape fractions of $\sim 20\%$–90%. Taking these into account, we do not regard the different f_{esc} values as a serious tension.

5.3. Limitations of this Study and Future Prospects

We discuss caveats and limitations of the relation between [O III]/[C II] and f_{esc}, then discuss how we can overcome the issues in the future. First, we derived an empirical relation between [O III]/[C II] and f_{esc} using (1) the known relation of f_{esc} and O$_{32}$ in Chisholm et al. (2018), and (2) the correlation of [O III]/[C II] and O$_{32}$ based on the combined sample of HDGS, LTS, and Mrk 54. Although the relation of f_{esc} and O$_{32}$ has been statistically confirmed in the latest study of Flury et al. (2022b), there exists a large scatter in the relation, not accurately traced by Equation (1). Second, the relation between [O III]/[C II] and f_{esc} can be severely affected by different selection functions adopted in the samples of local LCEs/non-LCEs in Chisholm et al. (2018) and the HDGS/LTS galaxies. Because there are only two known LCEs with the FIR line observations, Haro 11 and Mrk 54, however, we stress that the present study offers the best effort to empirically calibrate the relation of [O III]/[C II] and f_{esc}.

Clearly, a larger number of LCEs with FIR line observations is needed to refine the [O III]/[C II]–f_{esc} relation. Unfortunately, because of the closure of SOFIA, this kind of observation will be only possible with future FIR probes such as the PRobe Infrared Mission for Astrophysics (PRIMA), which will be able to target both [C II] and [O III] up to $z \sim 0.27$. Because some nearby LCEs at $z \sim 0.2$–0.4 have f_{esc} well beyond 10%, in contrast to the low values of Haro 11 and Mrk 54 ($f_{esc} \sim 2\%$–3%), such observations will be crucial to calibrate the [O III]/[C II]–f_{esc} relation up to the high f_{esc} regime. A better-calibrated relationship could be therefore a new powerful diagnostic tool to search for LCE candidates in addition to the current rest-frame UV/optical techniques.

Finally, we have assumed that the same relation between f_{esc} and [O III]/[C II] can be applied to high-z galaxies in Section 5.2. Although we do not have direct observations of rest-frame optical emission lines of these ALMA high-z galaxies, JWST will provide rest-frame optical emission lines of ALMA [O III] 88 μm emitters at $z \sim 6$–9 (e.g., GO1 #1840, PIs: J. Álvarez-Márquez and T. Hashimoto as well as GTO programs of #1776 PI: R. Windhorst, #1199 PI: M. Stiavelli,

#1262 PI: N. Luetzgendorf, and #1264 PI: L. Colina). With these data, it will be possible to test if the [O III]/[C II]–O_{32} relation holds at $z \sim 6$–9.

6. Summary

We presented SOFIA [C II] 158 μm and [O III] 88 μm observations of the local LCE, Mrk 54, at the luminosity distance of $\sim$191 Mpc. This is only the second LCE, after Haro 11, observed in the FIR lines, offering the opportunity to test if the [O III]/[C II] line luminosity ratio can be used as a tracer of f_{esc}, as proposed by Inoue et al. (2016) and Katz et al. (2020). Interestingly, we find that Mrk 54 has strong [C II] emission, whereas it has only moderate [O III] emission, resulting in the low [O III]/[C II] luminosity ratio of 0.22 ± 0.06. Combining Mrk 54 with the literature samples of the HDGS and LT surveys, we find that the [O III]/[C II] luminosity ratio correlates with O_{32}, sSFR, and FIR [O III]/[O I], and anticorrelates with the gas-phase metallicity in units of $12 + \log(O/H)$. The strongest correlations are found with O_{32} and FIR [O III]/[O I]. By combining the analytical form of f_{esc} and O_{32} in Chisholm et al. (2018) and the correlation between [O III]/[C II] and O_{32} found in this study, we obtain a relation between f_{esc} and [O III]/[C II]. The two confirmed LCEs, Haro 11 and Mrk 54, roughly follow the [O III]/[C II]–f_{esc} relation within uncertainties of 1σ and 2σ, respectively. If we assume that the same [O III]/[C II]–f_{esc} relation holds at high-z, galaxies with [O III]/[C II] $\gtrsim 7$ could have $f_{esc} \gtrsim 10\%$, significantly contributing to the reionization process. The presented multi-wavelength study will serve as an invaluable reference for ongoing and planned JWST observations of ALMA [O III] 88 μm emitters at high-z.

ORCID iDs

Takuya Hashimoto ⓘ https://orcid.org/0000-0002-0898-4038
Akio K. Inoue ⓘ https://orcid.org/0000-0002-7779-8677
Dario Fadda ⓘ https://orcid.org/0000-0002-3698-7076
Matthew Hayes ⓘ https://orcid.org/0000-0001-8587-218X
Johannes Puschnig ⓘ https://orcid.org/0000-0003-1111-3951
Erik Zackrisson ⓘ https://orcid.org/0000-0003-1096-2636
Yoichi Tamura ⓘ https://orcid.org/0000-0003-4807-8117
Hiroshi Matsuo ⓘ https://orcid.org/0000-0003-3278-2484
Ken Mawatari ⓘ https://orcid.org/0000-0003-4985-0201
Yoshinobu Fudamoto ⓘ https://orcid.org/0000-0001-7440-8832
Masato Hagimoto ⓘ https://orcid.org/0000-0001-8083-5814
Nario Kuno ⓘ https://orcid.org/0000-0002-1234-8229
Yuma Sugahara ⓘ https://orcid.org/0000-0001-6958-7856
Satoshi Yamanaka ⓘ https://orcid.org/0000-0002-7738-5290
Tom J. L. C. Bakx ⓘ https://orcid.org/0000-0002-5268-2221
Yurina Nakazato ⓘ https://orcid.org/0000-0002-0984-7713
Hidenobu Yajima ⓘ https://orcid.org/0000-0002-1319-3433
Naoki Yoshida ⓘ https://orcid.org/0000-0001-7925-238X

References

Algera, H., Inami, H., Sommovigo, L., et al. 2023, arXiv:2301.09659
Arata, S., Yajima, H., Nagamine, K., Li, Y., & Khochfar, S. 2019, MNRAS, 488, 2629
Asplund, M., Grevesse, N., Sauval, A. J., & Scott, P. 2009, ARA&A, 47, 481
Astropy Collaboration, Price-Whelan, A. M., Sipőcz, B. M., et al. 2018, AJ, 156, 123
Astropy Collaboration, Robitaille, T. P., Tollerud, E. J., et al. 2013, A&A, 558, A33
Bakx, T. J. L. C., Tamura, Y., Hashimoto, T., et al. 2020, MNRAS, 493, 4294
Bakx, T. J. L. C., Zavala, J. A., Mitsuhashi, I., et al. 2023, MNRAS, 519, 5076
Barrow, K. S. S., Robertson, B. E., Ellis, R. S., et al. 2020, ApJL, 902, L39
Begley, R., Cullen, F., McLure, R. J., et al. 2022, MNRAS, 513, 3510
Bergvall, N., Zackrisson, E., Andersson, B. G., et al. 2006, A&A, 448, 513
Borthakur, S., Heckman, T. M., Leitherer, C., & Overzier, R. A. 2014, Sci, 346, 216
Brauher, J. R., Dale, D. A., & Helou, G. 2008, ApJS, 178, 280
Carniani, S., Ferrara, A., Maiolino, R., et al. 2020, MNRAS, 499, 5136
Carniani, S., Maiolino, R., Pallottini, A., et al. 2017, A&A, 605, A42
Chisholm, J., Gazagnes, S., Schaerer, D., et al. 2018, A&A, 616, A30
Chisholm, J., Prochaska, J. X., Schaerer, D., Gazagnes, S., & Henry, A. 2020, MNRAS, 498, 2554
Chisholm, J., Saldana-Lopez, A., Flury, S., et al. 2022, MNRAS, 517, 5104
Cigan, P., Young, L., Cormier, D., et al. 2016, AJ, 151, 14
Cigan, P., Young, L. M., Gomez, H. L., et al. 2021, AJ, 162, 83
Colditz, S., Looney, L. W., Bigiel, F., et al. 2020, Proc. SPIE, 11453, 1145334
Cormier, D., Lebouteiller, V., Madden, S. C., et al. 2012, A&A, 548, A20
Cormier, D., Madden, S. C., Lebouteiller, V., et al. 2015, A&A, 578, A53
de Barros, S., Vanzella, E., Amorín, R., et al. 2016, A&A, 585, A51
De Looze, I., Cormier, D., Lebouteiller, V., et al. 2014, A&A, 568, A62
Decarli, R., Pensabene, A., Venemans, B., et al. 2022, A&A, 662, A60
Deharveng, J. M., Buat, V., Le Brun, V., et al. 2001, A&A, 375, 805
Dijkstra, M., Gronke, M., & Venkatesan, A. 2016, ApJ, 828, 71
Eggen, N. R., Scarlata, C., Skillman, E., & Jaskot, A. 2021, ApJ, 912, 12
Fadda, D., & Chambers, E. T. 2018, AAS Meeting, 231, 150.11
Ferland, G. J., Porter, R. L., van Hoof, P. A. M., et al. 2013, RMxAA, 49, 137
Finkelstein, S. L., D'Aloisio, A., Paardekooper, J.-P., et al. 2019, ApJ, 879, 36
Fischer, C., Beckmann, S., Bryant, A., et al. 2018, JAI, 7, 1840003
Fletcher, T. J., Tang, M., Robertson, B. E., et al. 2019, ApJ, 878, 87
Flury, S. R., Jaskot, A. E., Ferguson, H. C., et al. 2022a, ApJS, 260, 1
Flury, S. R., Jaskot, A. E., Ferguson, H. C., et al. 2022b, ApJ, 930, 126
Fujimoto, S., Ouchi, M., Ferrara, A., et al. 2019, ApJ, 887, 107
Harikane, Y., Ouchi, M., Inoue, A. K., et al. 2020, ApJ, 896, 93
Hashimoto, T., Inoue, A. K., Mawatari, K., et al. 2019, PASJ, 71, 71
Hashimoto, T., Laporte, N., Mawatari, K., et al. 2018, Natur, 557, 392
Hayes, M., Östlin, G., Atek, H., et al. 2007, MNRAS, 382, 1465
Hayes, M., Östlin, G., Schaerer, D., et al. 2013, ApJL, 765, L27
Helou, G., Soifer, B. T., & Rowan-Robinson, M. 1985, ApJL, 298, L7
Henry, A., Berg, D. A., Scarlata, C., Verhamme, A., & Erb, D. 2018, ApJ, 855, 96
Herrera-Camus, R., Sturm, E., Graciá-Carpio, J., et al. 2018, ApJ, 861, 95
Hunter, D. A., Ficut-Vicas, D., Ashley, T., et al. 2012, AJ, 144, 134
Inoue, A. K., & Iwata, I. 2008, MNRAS, 387, 1681
Inoue, A. K., Iwata, I., & Deharveng, J.-M. 2006, MNRAS, 371, L1

Inoue, A. K., Iwata, I., Deharveng, J. M., Buat, V., & Burgarella, D. 2005, A&A, 435, 471
Inoue, A. K., Tamura, Y., Matsuo, H., et al. 2016, Sci, 352, 1559
Iwata, I., Inoue, A. K., Matsuda, Y., et al. 2009, ApJ, 692, 1287
Iwata, I., Inoue, A. K., Micheva, G., Matsuda, Y., & Yamada, T. 2019, MNRAS, 488, 5671
Izotov, Y. I., Orlitová, I., Schaerer, D., et al. 2016a, Natur, 529, 178
Izotov, Y. I., Schaerer, D., Thuan, T. X., et al. 2016b, MNRAS, 461, 3683
Izotov, Y. I., Schaerer, D., Worseck, G., et al. 2018, MNRAS, 474, 4514
Jaskot, A. E., & Oey, M. S. 2013, ApJ, 766, 91
Jones, L. H., Barger, A. J., & Cowie, L. L. 2021, ApJ, 908, 222
Jones, T. A., Ellis, R. S., Schenker, M. A., & Stark, D. P. 2013, ApJ, 779, 52
Kakiichi, K., & Gronke, M. 2021, ApJ, 908, 30
Katz, H., Galligan, T. P., Kimm, T., et al. 2019, MNRAS, 487, 5902
Katz, H., Rosdahl, J., Kimm, T., et al. 2022, MNRAS, 510, 5603
Katz, H., Ďurovčíková, D., Kimm, T., et al. 2020, MNRAS, 498, 164
Kohandel, M., Ferrara, A., Pallottini, A., et al. 2023, MNRAS, 520, L16
Komatsu, E., Smith, K. M., Dunkley, J., et al. 2011, ApJS, 192, 18
Laporte, N., Ellis, R. S., Boone, F., et al. 2017, ApJL, 837, L21
Laporte, N., Katz, H., Ellis, R. S., et al. 2019, MNRAS, 487, L81
Leitet, E., Bergvall, N., Hayes, M., Linné, S., & Zackrisson, E. 2013, A&A, 553, A106
Leitet, E., Bergvall, N., Piskunov, N., & Andersson, B. G. 2011, A&A, 532, A107
Leitherer, C., Hernandez, S., Lee, J. C., & Oey, M. S. 2016, ApJ, 823, 64
Lord, S. D. 1992, NASA Technical Memorandum, 103957, NASA
Ma, X., Kasen, D., Hopkins, P. F., et al. 2015, MNRAS, 453, 960
Ma, X., Quataert, E., Wetzel, A., et al. 2020, MNRAS, 498, 2001
Madden, S. C., Rémy-Ruyer, A., Galametz, M., et al. 2013, PASP, 125, 600
Marques-Chaves, R., Schaerer, D., Álvarez-Márquez, J., et al. 2021, MNRAS, 507, 524
Marques-Chaves, R., Schaerer, D., Alvarez-Marquez, J., et al. 2022, MNRAS, 517, 2972
Meijerink, R., Spaans, M., & Israel, F. P. 2007, A&A, 461, 793
Micheva, G., Iwata, I., Inoue, A. K., et al. 2017, MNRAS, 465, 316
Moriwaki, K., Yoshida, N., Shimizu, I., et al. 2018, MNRAS, 481, L84
Naidu, R. P., Matthee, J., Oesch, P. A., et al. 2022, MNRAS, 510, 4582
Nakajima, K., & Ouchi, M. 2014, MNRAS, 442, 900
Nakazato, Y., Yoshida, N., & Ceverino, D. 2023, arXiv:2301.02416
Nestor, D. B., Shapley, A. E., Kornei, K. A., Steidel, C. C., & Siana, B. 2013, ApJ, 765, 47
Nestor, D. B., Shapley, A. E., Steidel, C. C., & Siana, B. 2011, ApJ, 736, 18

Paardekooper, J.-P., Khochfar, S., & Dalla Vecchia, C. 2015, MNRAS, 451, 2544
Pahl, A. J., Shapley, A., Steidel, C. C., Chen, Y., & Reddy, N. A. 2021, MNRAS, 505, 2447
Puschnig, J., Hayes, M., Östlin, G., et al. 2017, MNRAS, 469, 3252
Puschnig, J., Hayes, M., Östlin, G., et al. 2020, A&A, 644, A10
Ramambason, L., Lebouteiller, V., Bik, A., et al. 2022, A&A, 667, A35
Rémy-Ruyer, A., Madden, S. C., Galliano, F., et al. 2013, A&A, 557, A95
Ren, Y. W., Fudamoto, Y., Inoue, A. K., et al. 2023, ApJ, 945, 69
Rivera-Thorsen, T. E., Hayes, M., & Melinder, J. 2022, A&A, 666, A145
Robertson, B. E. 2022, ARA&A, 60, 121
Robertson, B. E., Furlanetto, S. R., Schneider, E., et al. 2013, ApJ, 768, 71
Rosdahl, J., Blaizot, J., Katz, H., et al. 2022, MNRAS, 515, 2386
Saha, K., Tandon, S. N., Simmonds, C., et al. 2020, NatAs, 4, 1185
Saxena, A., Pentericci, L., Ellis, R. S., et al. 2022a, MNRAS, 511, 120
Saxena, A., Cryer, E., Ellis, R. S., et al. 2022b, MNRAS, 517, 1098
Schaerer, D., Izotov, Y. I., Worseck, G., et al. 2022, A&A, 658, L11
Shapley, A. E., Steidel, C. C., Strom, A. L., et al. 2016, ApJL, 826, L24
Smirnova-Pinchukova, I., Husemann, B., Busch, G., et al. 2019, A&A, 626, L3
Sommovigo, L., Ferrara, A., Carniani, S., et al. 2021, MNRAS, 503, 4878
Steidel, C. C., Bogosavljević, M., Shapley, A. E., et al. 2018, ApJ, 869, 123
Sugahara, Y., Inoue, A. K., Fudamoto, Y., et al. 2022, ApJ, 935, 119
Tamura, Y., Mawatari, K., Hashimoto, T., et al. 2019, ApJ, 874, 27
Vacca, W., Clarke, M., Perera, D., Fadda, D., & Holt, J. 2020, in ASP Conf. Ser. 527, Astronomical Data Analysis Software and Systems XXIX, ed. R. Pizzo et al. (San Francisco, CA: ASP), 547
Vallini, L., Ferrara, A., Pallottini, A., Carniani, S., & Gallerani, S. 2021, MNRAS, 505, 5543
Vallini, L., Ferrara, A., Pallottini, A., & Gallerani, S. 2017, MNRAS, 467, 1300
Vanzella, E., Nonino, M., Cupani, G., et al. 2018, MNRAS, 476, L15
Vanzella, E., Siana, B., Cristiani, S., & Nonino, M. 2010, MNRAS, 404, 1672
Verhamme, A., Orlitová, I., Schaerer, D., & Hayes, M. 2015, A&A, 578, A7
Virtanen, P., Gommers, R., Oliphant, T. E., et al. 2020, NatMe, 17, 261
Walter, F., Riechers, D., Novak, M., et al. 2018, ApJL, 869, L22
Wang, B., Heckman, T. M., Leitherer, C., et al. 2019, ApJ, 885, 57
Witstok, J., Smit, R., Maiolino, R., et al. 2022, MNRAS, 515, 1751
Wolfire, M. G., Vallini, L., & Chevance, M. 2022, ARA&A, 60, 247
Yajima, H., Choi, J.-H., & Nagamine, K. 2011, MNRAS, 412, 411
Yajima, H., Li, Y., Zhu, Q., et al. 2014, MNRAS, 440, 776
Yamanaka, S., Inoue, A. K., Yamada, T., et al. 2020, MNRAS, 498, 3095
Yeh, J. Y. C., Smith, A., Kannan, R., et al. 2023, MNRAS, 520, 2757
Zackrisson, E., Inoue, A. K., & Jensen, H. 2013, ApJ, 777, 39